Osteoarthritis and Cartilage

International Cartilage Repair Society

I C R S

OARSI OSTEOARTHRITIS RESEARCH SOCIETY INTERNATIONAL

Novel optical imaging technique to determine the 3-D orientation of collagen fibers in cartilage: variable-incidence angle polarization-sensitive optical coherence tomography

N. Ugryumova Ph.D., J. Jacobs M.Eng., M. Bonesi M.S. and S. J. Matcher Ph.D.*
Department of Engineering Materials, University of Sheffield, Mappin Street, Sheffield S1 3JD, UK

Summary

Objective: To investigate a novel optical method to determine the three dimensional (3-D) structure of articular cartilage collagen non-destructively.

Methods: Polarization-sensitive optical coherence tomography was used to determine the apparent optical birefringence of articular cartilage for a number of different illumination directions. A quantitative method based on the theory of light propagation in uniaxial crystalline materials was validated on equine flexor tendon. Qualitative maps of fiber polar and azimuthal orientation at sites on the posterior and anterior segments of the equine third metacarpophalangeal (fetlock) joint were produced, and the azimuthal orientations compared with data from a split-line experiment.

Results: Polar and azimuthal angles of cut flexor tendon broadly agreed with the nominal values but suggested that the accuracy was limited by our method of determining the apparent birefringence. On intact equine fetlock joints we found a non-zero polar tilt that changed in direction at various points along the apex, moving from the sagittal ridge outwards. The azimuthal orientation changes from being parallel to the sagittal ridge in the posterior region to being inclined to the ridge in the anterior region. This broadly agrees with split-line data for the anterior region but differs in the posterior region, possibly reflecting depth-dependent orientation changes.

Conclusion: General quantitative agreement was found between our method and histology in validation experiments. Qualitative results for cartilage suggest a complicated 3-D structure that warrants further study. There is potential to develop this approach into a tool that can provide depth-resolved information on collagen orientation in near real-time, non-destructively and *in vivo*.
© 2008 Osteoarthritis Research Society International. Published by Elsevier Ltd. All rights reserved.

Key words: Polarization-sensitive OCT, Collagen, Birefringence, Cartilage, Osteoarthritis, Tissue engineering.

Introduction

Osteoarthritis is generally recognized to involve a degradation of the extracellular matrix (ECM) in articular cartilage. Treatments include osteochondral autograft, autologous chondrocyte implantation and tissue engineering of replacement cartilage tissue[1]. Unfortunately many tissue-engineered cartilage constructs display poor adhesion to the surrounding native cartilage, leading to poor mechanical performance when exposed to *in vivo* stresses[2]. Since the primary supplier of tensile strength is type-II collagen, it is likely that the organization of collagen fibers at a given location is strongly related to the mechanical demands existing at that site. Evidence exists that the superficial layer, containing fibers oriented parallel to the surface, is important for distributing applied compressive loads over a larger volume of tissue, for example[3]. Consequently it has been proposed that improved mechanical performance will result from ensuring that the collagen matrix regenerates to a morphologically similar state as existed in the original tissue and that, in tissue-engineered constructs, this could be achieved by the application of a suitable mechanical stimulus[4]. To further this end, methods that could assess the three dimensional (3-D) organization of cartilage collagen *in situ* are potentially valuable.

A number of methods exist to determine collagen orientation. The simplest method is the "split-line" technique, in which the cartilage tissue is pricked with a needle and then splits along the direction of collagen alignment[5]. Obviously this technique is destructive and laborious. Small angle X-ray scattering (SAXS) is powerful but cannot be used *in vivo* and lacks depth-penetration or intrinsic depth-sectioning[6]. Its use, therefore, is confined to histological sections. Recent advances in magnetic resonance imaging, especially diffusion-tensor imaging, now allow non-destructive determination of the 3-D orientation of collagen fibers in cartilage[7]. However, the method is too slow (hours per volume image) to apply *in vivo* and too expensive to be deployed routinely in, for example, a bioreactor. Also, the voxel size is typically around 100 μm, which is comparable to the length scale on which cartilage shows large variations in collagen organization (the superficial layer is typically about 100 μm thick).

Many biological tissues exhibit strong linear optical birefringence, particularly those whose main constituent is collagen. Hence polarized light microscopy, especially in conjunction with Sirius Red staining, has been used for

*Address correspondence and reprint requests to: Dr S. J. Matcher, Ph.D., Department of Engineering Materials, University of Sheffield, Mappin Street, Sheffield S1 3JD, UK. Tel: 44-114-2225994; Fax: 44-114-2225945; E-mail: s.j.matcher@sheffield.ac.uk

decades to determine the collagen orientation from measurements of the birefringence fast-axis orientation[8]. However, the method is destructive and gives definitive information only on fiber orientation within the plane of sectioning. More recently, polarized fourier transform infrared (FTIR) imaging has proven successful in determining collagen fiber orientations[9]. Again, however, FTIR imaging is limited to imaging the exposed surface of cut tissue, because of the low penetration of mid-IR light into biological tissue. It could not be used to remotely interrogate cultured tissues that were immersed in an aqueous environment. Hence there is a need for a tool that can yield high-resolution 3-D information cheaply, rapidly, non-destructively and remotely.

In recent years polarization-sensitive optical coherence tomography (OCT) (PS-OCT) has emerged as a powerful means to image tissue birefringence *in vivo*, with reported applications in studying burn depths in skin[10], characterizing osteoarthritic changes in articular cartilage[11] and studying the variation of fiber orientation with depth in muscle[12] and intervertebral disk[21]. PS-OCT is derived from OCT, which can be thought of as an optical analog of ultrasound (US) imaging. Unlike US, OCT has lower tissue penetration (≤ 1 mm depending on tissue type and optical wavelength used) but much higher spatial resolution (<2 μm axial resolution has been demonstrated and 20 μm lateral resolution is typical). Over the last decade, OCT has established itself as the method of choice for retinal imaging *in vivo*[13] and is attracting interest in many biomedical applications including tissue engineering[14]. OCT generates its image contrast in the same manner as US imaging, i.e., it identifies tissue boundaries. It has shown promise as a tool for studying the *in situ* development of cartilage allografts in a rabbit model of osteoarthritis[15]. PS-OCT extends the performance of OCT by adding a new contrast mechanism: tissue birefringence.

Previous reports on the use of PS-OCT have concentrated on situations in which the fibers are oriented so as always to lie parallel to the tissue surface. In this case it is only necessary to determine the 'fast-axis' orientation, which corresponds to the azimuthal orientation of the collagen fiber (since collagen is technically a 'positive uniaxial' material, the fast-axis lies at $90°$ to the long-axis of the fibers). However, in cartilage it is well known from histology that this is not the case, with fibers showing a large variation in their polar angle with depth. The polar angle (measured relative to the surface normal), ranges from $90°$ in the superficial layer to around $0°$ in the radial layer, where the fibers then meet the tide-mark. In the intervening transitional layer the fibers have an intermediate and less ordered orientation[9].

In order to determine the fiber polar angle, we previously introduced a method of imaging the tissue using a series of angle-dependant measurements for a given location on the surface[16]. It is known from the optics of uniaxial birefringent materials that if light propagates along the optic axis (i.e., the '*c*-axis' in optical terminology), then the sample displays no birefringence whereas if the light beam travels orthogonal to the *c*-axis then the observed birefringence reaches its maximum value[17]. It is generally assumed that this *c*-axis corresponds to the long-axis of the collagen fibers in birefringent biological tissues[8]. We, therefore, crudely determined the 3-D collagen orientation by determining the illumination direction that apparently yielded zero birefringence. A further development was to make this method quantitative, by exploiting the known theoretical relationship between the "apparent" birefringence, the "true" birefringence (this latter quantity being an intrinsic optical property of the tissue, determined by the density and spatial ordering of collagen fibrils, the refractive index of the ground substance, etc.[18]) and the angle between the *c*-axis and the light propagation direction[19]. This simplified method used illumination directions confined to a single-plane and assumed that the fibers were inclined only in this plane, i.e., it was effectively assumed that the azimuthal angle was zero. This simple quantitative approach was validated by determining the polar angle of fibers in a cut piece of equine flexor tendon.

In this report we extend the method to infer full 3-D information by relaxing this assumption and adding measurements for incident beams that are inclined in two orthogonal planes.

Methods

All measurements were conducted on *ex vivo* tissue samples taken from horses destined for the human food chain. Intact forelimbs were obtained from a local abattoir, operated in accordance with relevant legislation.

ARTICULAR CARTILAGE SAMPLES

Tissue samples were taken from the equine fetlock joint, which permits rotation in the sagittal plane between the proximal phalanx and the third metacarpal bone. This joint often displays osteoarthritic lesions, probably because of the relatively small contact area available at this joint for the transmission of the ground reaction force during running on hard surfaces.

Intact equine forelimbs were dissected to separate the third metacarpal from the proximal phalanx. The condyle of the third metacarpal was then isolated by sawing away and discarding most of the shaft. Fig. 1. shows a photograph of the tissue preparation, prior to imaging. The condyles, with intact cartilage attached, were then either imaged fresh or stored in a $-80°C$ freezer for subsequent defrosting and imaging. During imaging, the samples were maintained moist by application of 0.15 M NaCl during measurements. In several experiments, the angle between the cartilage surface and the probe beam was varied in two orthogonal planes. This was achieved by mounting the specimen on a system of two graduated rotation stages, whose positions were adjusted as a function of inclination angle, in order to image a fixed site on the surface and whose axes of rotation allowed rotation of the joint surface in these planes.

POLARIZATION OCT SYSTEM

Several excellent reviews of the PS-OCT technique can be found in the optics literature[20]. Our polarization-sensitive low-coherence interferometer design has been described in detail elsewhere[21]. Briefly, light from a 0.9 mW, 1.3 μm broad-band superluminescent diode (SLD) light-source is vertically polarized and launched into a bulk-optics PS-OCT interferometer. Visible light from a 635 nm laser diode is coupled into the SLD output

Fig. 1. Photograph illustrating the equine third metacarpophalangeal joint. The sagittal ridge is clearly seen in the middle of the condyle (end of left-most bone).

fiber using a 90:10 2×1 coupler, thus aiding visualization of the near-infrared sample beam on the tissue surface. A non-polarizing beam splitter diverts 50% of the light into the sample arm, where it is passed through a quarter-wave plate, with fast-axis at 45° to the vertical, thus illuminating the sample with circularly polarized light. The sample light is focused onto the specimen using a 0.10 NA microscope objective, yielding a transverse resolution of approximately 20 μm full width at half maximum (FWHM). The reference arm light is passed through a quarter-wave plate and variable neutral density filter[22] before entering a scanning optical delay. Movement of the mirror in this delay line allows us to acquire a single OCT A-scan, analogous to an US A-scan. A two-dimensional (2-D) cross-sectional images (i.e., an OCT 'B-scan') is built up by collecting multiple A-scans whilst laterally scanning the sample using a motor stage.

After interferometric recombination with the back-scattered sample beam, the light is split into horizontally and vertically polarized components using a polarizing beam splitter. Two OCT depth-resolved interferograms, one for the horizontal and one for the vertical polarized light components, are then detected by two identical photoreceivers, amplified and then digitized by an analog-to-digital converter card hosted by a PC. Standard OCT signal processing is then applied[23] which produces demodulated A-scans for the two orthogonal polarization states. Denoting the amplitudes of the demodulated signals for the vertical and horizontal polarization components as $A_v(z)$ and $A_h(z)$, respectively, where z is physical depth into the sample, then Hee et al. showed that the depth-resolved cumulative single-pass retardance δ (i.e., the phase-difference between the horizontal and vertical electric field components that is accumulated by the light beam in propagating to a given depth in the medium) can be calculated using the following formula[24]:

$$\delta(z) = \tan^{-1}(A_v(z)/A_h(z)). \tag{1}$$

The retardance is related to a more fundamental quantity, which we will term the "apparent birefringence" Δn by the formula:

$$\delta(z) = z\left(\frac{2\pi\Delta n}{\lambda_0}\right), \tag{2}$$

where λ_0 is the wavelength of the light in air. NB this formula is a simplified version which assumes that Δn does not vary with depth z. Since both $A_v(z)$ and $A_h(z)$ are always positive, in this simple PS-OCT approach δ will be determined modulo $\pi/2$ radians. Hence for a tissue with uniform Δn, PS-OCT yields 2-D cross-sectional images of δ (i.e., "retardance images") that have a banded appearance with respect to depth z. The band-spacing d represents the distance z over which δ increases from 0 to π and so can be used to infer Δn using the equation:

$$\Delta n = \frac{\lambda_0}{2d} \tag{3}$$

hence the band-spacing in a PS-OCT retardance image gives a simple way to infer Δn.

However, there are situations in which this method may not be applicable, in particular in weakly birefringent media the retardation band may be so broad that its full extent cannot be discerned from the OCT image (the typical useable depth of which in cartilage is 0.7−1 mm). In this case one can try to determine the birefringence by measuring the slope of the retardance δ with respect to z, i.e., using the equation:

$$\Delta n = \frac{\lambda_0}{2\pi}\frac{d\delta(z)}{dz}. \tag{4}$$

This approach has the advantage that Δn can be estimated for weakly birefringent tissues such as cartilage, where a complete birefringence band may not be visible. It has the additional advantage that depth-dependent variations in Δn can be detected because $\delta(z)$ vs z will not be a straight line. However, in our experience it has the disadvantage that it tends to underestimate Δn. The reason for this is illustrated in Fig. 2. The origin of Eq. (1) is that one can show that the vertically and horizontally polarized interference amplitudes A_v and A_h oscillate with increasing depth according to the relation (in the ideal case)[20]

$$A_v(z) = \sin\left(\frac{2\pi}{\lambda_0}\Delta nz\right) \quad A_h(z) = \cos\left(\frac{2\pi}{\lambda_0}\Delta nz\right). \tag{5}$$

In the absence of phase-resolved information only the magnitudes of A_v and A_h are determined hence $\delta(z)$ ideally starts at zero at $z = 0$ (when $A_v = 0$), then increases uniformly to a peak value of $\pi/2$ (at $z = \lambda_0/4\Delta n$, hence $A_h = 0$) until falling uniformly back to zero. This pattern then repeats indefinitely. In reality, however, (1) the amplitudes of the back-scattered fields falls exponentially with depth with a decay constant μ_t and (2) the measurements will always include background noise terms due to for example system measurement noise and also multiply back-scattered and randomly polarized
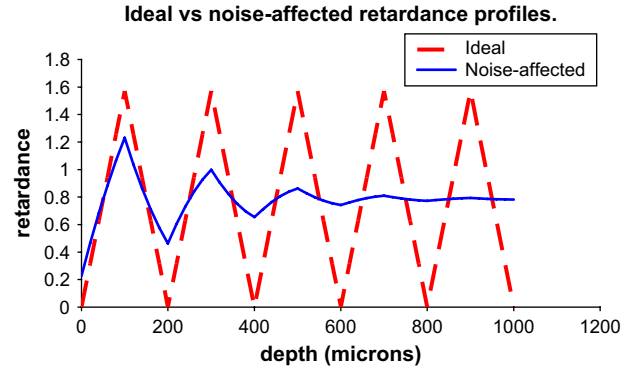

Ideal vs noise-affected retardance profiles.

Fig. 2. A comparison between the ideal and actual (i.e., "noise-affected") depth-resolved retardance curves for a uniformly birefringent material such as tendon. Note how the gradient of the actual retardance profile systematically underestimates the gradient of the "ideal" curve and hence produces an estimate of Δn that is lower than that inferred from the band-spacing.

light. Hence A_v and A_h can never truly fall to zero and so δ never fully achieves the values of zero and $\pi/2$. This effect becomes more pronounced with increasing depth. The "noise-affected" curve in Fig. 2 is generated by modifying Eq. (5) to the form:

$$A_v(z) = \sin\left(\frac{2\pi}{\lambda_0}\Delta nz\right)\exp(-2\mu_t z) + \sigma$$

$$A_h(z) = \cos\left(\frac{2\pi}{\lambda_0}\Delta nz\right)\exp(-2\mu_t z) + \sigma \tag{6}$$

where σ is a noise-bias term.

For either method of determining Δn, speckle noise was reduced by typically averaging 25 lateral A-scans are to produce the graph of retardance vs depth. Normal incidence of the OCT light beam onto the tissue surface was determined by maximizing the strength of the Fresnel reflection from the air/tissue interface. Rotation of the sample through a known angle was thus made relative to this known starting point.

DETERMINATION OF 3-D FIBER ORIENTATION: THEORY

To describe the birefringence displayed by cartilage tissue with an arbitrary 3-D orientation of the collagen fibers, the tissue was modeled as a positive uniaxial birefringent crystal structure. As noted above, if light propagates along the c-axis of such a medium then the sample displays no birefringence whereas if the light beam travels orthogonal to the fiber long-axis then the observed birefringence reaches its maximum value. More quantitatively, it is well known[17] that if an optical plane wave propagates through this material with angle θ_c between the direction of propagation and the c-axis then two orthogonal polarization eigenmodes exist which experience refractive indices n_o and n, respectively, where n is given by,

$$\frac{1}{n^2} = \frac{\sin^2\theta_c}{n_e^2} + \frac{\cos^2\theta_c}{n_o^2}, \tag{7}$$

where n_o is the "ordinary" and n_e the "extraordinary" refractive index. This motivates us to define the apparent birefringence as $\Delta n = n - n_o$ and the true birefringence as $n_e - n_o$. Clearly, the true birefringence of the tissue is the more fundamental quantity, whereas the apparent birefringence is determined by the true birefringence and geometric factors. The two quantities are related by:

$$\Delta n = n_o\left(\frac{n_e}{\sqrt{n_o^2 + \cos^2(\theta_c)(n_e^2 - n_o^2)}} - 1\right). \tag{8}$$

Our method involves determining Δn using PS-OCT retardance images for a set of different illumination directions. In a previous paper[19] we described a method to determine the polar angle of the optic axis of a uniaxial birefringent biological tissue quantitatively by making PS-OCT measurements with a number of incident illumination directions and hence different values of θ_c[19]. By assuming a value for n_o, the simultaneous solution of a set of Eq. (8) yields best-estimates for the unknown polar orientation and
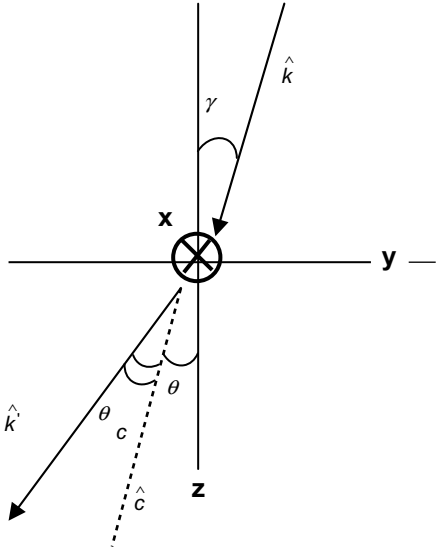
Fig. 3. Refraction of light between an isotropic (top) and uniaxially anisotropic (bottom) media.

extraordinary refractive index n_e. The method was validated on equine flexor tendon, yielding a variability of 4% for the true birefringence and 3% for the polar angle. However, this method assumed that the optic axis lay in a given plane and that the illumination directions lay in this same plane.

In this paper we again model biological tissue as a uniaxial crystal and solve for the orientation of the c-axis in 3-D space. The simple analysis presented here assumes that the c-axis has a non-zero azimuthal angle φ, in addition to a polar angle θ different from 90° and that both of these parameters stay constant with depth.

Let the plane of incidence with azimuthal angle $\varphi = 0$ be the y–z plane. Then k_{oz} and k_{ez} are the z-components of the ordinary and extraordinary wave vector, respectively. Hence the incident ordinary and extraordinary wave vectors can be written as:

$$\mathbf{k}_o = \beta \widehat{y} + k_{oz} \widehat{z} \quad \mathbf{k}_e = \beta \widehat{y} + k_{ez} \widehat{z}. \tag{9}$$

A similar result applies when the plane of incidence is the x–z plane, i.e., the azimuthal angle $\varphi = 90°$.

Here β is the tangential component of the incident wave vector and is conserved during refraction across a plane interface[17].

On entering the tissue, Snell's law of refraction implies that the transmitted wave vector (denoted by primed symbols) becomes (Fig. 3):

$$\widehat{k}' = \sin \gamma' \cdot \widehat{y} + \cos \gamma' \cdot \widehat{z} = \frac{\sin \gamma}{n_0} \cdot \widehat{y} + \left(1 - \frac{\sin^2 \gamma}{n_0^2}\right)^{\frac{1}{2}} \cdot \widehat{z} \tag{10}$$

for the y–z plane of incidence, where γ' $(=\theta + \theta_c)$ is the polar angle of the transmitted wave vector. Let the direction of the c-axis in 3-D space be defined by a unit vector $\widehat{c}$ in spherical polar co-ordinates (θ, φ)[25]:

$$\widehat{c} = \left(\widehat{x}. \sin \varphi + \widehat{y}. \cos \varphi\right) \sin \theta + \widehat{z}. \cos \theta \tag{11}$$

From Fig. 3 we see that $\cos \theta_c = \widehat{c} \cdot \widehat{k}'$ and so when the plane of incidence is the y–z plane then applying Eqs. (10) and (11) we have:

$$\cos \theta_{c1} = \cos \varphi \cdot \sin \theta \cdot \sin \gamma' + \cos\theta \cdot \cos\gamma' \tag{12}$$

A similar result holds for the x–z plane of incidence.

If a value for n_o is assumed or measured then substituting Eq. (12) and its equivalent into Eq. (8) for measurements in two orthogonal planes, respectively, yields relationships between the apparent birefringence Δn, the angle of illumination γ and the three unknown parameters φ, θ and n_e. Simultaneous solution of the resulting system of equations using measured values of Δn for different values of γ can then yield estimates for these unknowns. We obtain best-estimates for φ, θ and n_e from an over-constrained problem by performing a three-variable minimization of the error-metric

$$\chi^2 = \sum_{i=1}^{10} \left(\Delta n_{i,\text{measured}} - \Delta n_{i,\text{predicted}}\right)^2, \tag{13}$$

where the ten measurements correspond to five illumination directions for each of the two orthogonal planes of incidence.

Results

VALIDATION EXPERIMENTS − I

To investigate the accuracy of our method to quantitatively characterize the 3-D orientation of the optical c-axis in biological tissues a series of measurements on tendon tissue were made. A sample of equine flexor tendon was cut, whilst frozen, such that the c-axis was oriented at a polar angle of approximately 20°, as judged by a digital photograph. Then the sample was rotated in a holder to produce an azimuthal angle $\varphi \approx 30°$. The surface of the cut was illuminated at normal incidence and by clockwise and anticlockwise angle sequences $\pm 20°$, $\pm 40°$ in two orthogonal planes of incidence. Measurements of apparent birefringence were made in all cases by taking profiles through the resulting retardance images and measuring
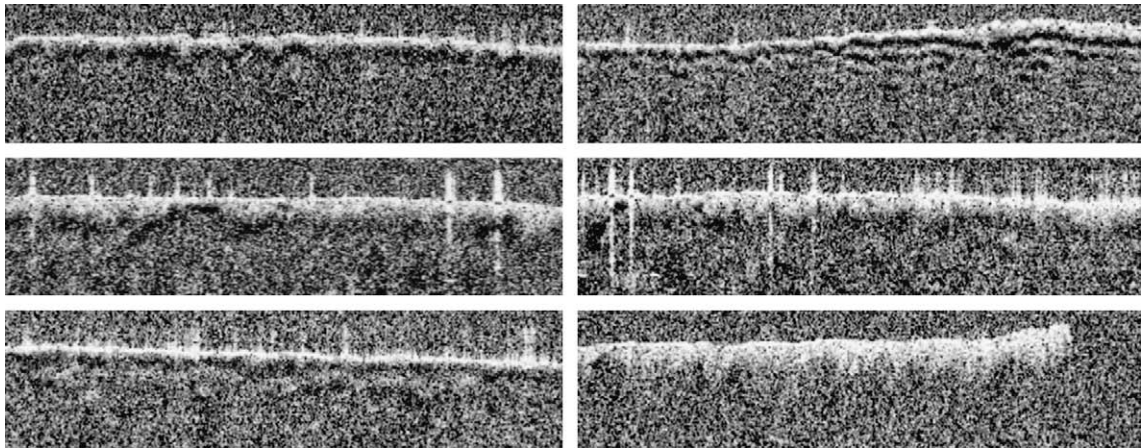

Fig. 4. Retardance images obtained from a tendon sample cut such that $\theta = 20°$ and $\varphi = 0°$ (i.e., collagen fibers oriented so as to run vertically in the lab frame). Δn is consequently low and hence a full birefringence band is not evident for many angles of illumination. Left column: illumination directions lying in the laboratory horizontal plane with polar angles of $-40°$, $0°$ and $+40°$, respectively. Right column: ditto for the vertical plane. As can be seen, it is impossible to infer Δn from the band-spacing for most of these images, however, it can be inferred from the curve of retardance vs depth.

Table I

Best-estimates of the true birefringence $n_e - n_o$, fiber polar angle θ and azimuthal angle φ of a sample of tendon cut to possess nominal parameters $\theta_{nominal}$ and $\varphi_{nominal}$. Each row reports results obtained using incidence angles of $-20°$, $+20°$, $0°$, $-40°$, and $+40°$ for the light beam in both orthogonal planes

Sample number	$n_e - n_o$	$\theta_{derived}$ (°)	$\theta_{nominal}$ (°)	$\theta_{adjusted}$ (°)	$\varphi_{derived}$ (°)	$\varphi_{nominal}$ (°)	$\varphi_{adjusted}$ (°)	χ^2 (min)
1	5.3×10^{-3}	76.6	73	75.7	34	33	35	2.6×10^{-6}
2	5.4×10^{-3}	78.6	69	72.2	38	31	32.1	5.3×10^{-7}
3	4.7×10^{-3}	79.3	63.5	66.7	31	33	31	1.4×10^{-6}

the physical spacing d of the retardance bands for each illumination direction (an ordinary tissue refractive index of $n_o = 1.4$ was assumed in order to convert optical path into physical path). Sets of five measurements of Δn vs γ were then compiled and the error-metric χ^2 minimized w.r.t. $n_e - n_o$, θ and φ using the Nelder-Mead simplex algorithm (Matlab® function fminsearch), using an initial guess for $n_e - n_o$ equal to the largest Δn in the measurement set, the initial θ equal to that γ' in the set which yields the smallest Δn and the initial φ equal to 0 or 90° depending on whether the widest retardance band occurred for the $y-z$ or $x-z$ plane of incidence.

Table I lists the resulting estimates for $n_e - n_o$, θ, φ and also the minimum χ^2 achieved by the simplex algorithm for various samples. All samples had nominal polar fiber orientation approximately $65-75°$ ($\theta_{nominal}$) and $30-35°$ nominal azimuthal angle ($\varphi_{nominal}$), as measured by a digital photograph. The incident light beam was oriented normal to the surface and at different incident angles $\pm 20°$, $\pm 40°$ for two orthogonal planes.

For the first sample the derived value of θ ($\theta_{derived}$) was within 4% of the nominal value and the derived value of φ was within 5% of the nominal value. However, the difference for the second and third samples was larger. The derived value of the polar angle fluctuates by 10 and 5% and the value for azimuthal angle is within 3 and 5% of the nominal value, respectively.

Our estimated experimental uncertainty in determining the retardance band-spacing is about 10%. By manually adjusting the retardance bands spacing within this tolerance, i.e., by about 10% we could derive polar and azimuthal angles for all samples within about 2% of their nominal values (columns $\theta_{adjusted}$ and $\varphi_{adjusted}$ list the values). This suggests that our method is currently limited by our accuracy in determining the retardance band-spacing. Often the bands were rather indistinct. We are currently working to improve the data collection procedure for retardance images and to improve the precision of the algorithm of birefringence calculations using Jones matrix methods[12].

VALIDATION EXPERIMENTS — II

In some situations (for example when θ or $n_e - n_o$ are small) then Δn is too small for a complete birefringence band to be formed, for many of the illumination directions. To explore this case, we extended the method to make use of Δn derived using Eq. (4). A sample of tendon was cut with a polar angle of 20° and adjusted so that $\Phi = 0°$, then retardance images were collected in the usual way (see Fig. 4). It is evident that it is not possible to infer the band-spacing from most of these images, however, Δn can be extracted using Eq. (4) (Fig. 5). Table II summarizes the results of the tendon experiments comparing the method used in Table I with that based on Eq. (4). The last row reports results for the data shown in Fig. 4, i.e., where the method used in Table I cannot be applied, due to the absence of a complete retardance band. Note that where the two methods are compared, the fiber orientation information is in good agreement but the true birefringence is underestimated by the gradient-based method. This shows that careful calibration of noise-bias effects are needed if accurate birefringence measurements are to be obtained using PS-OCT deep in scattering tissues.

ARTICULAR CARTILAGE COLLAGEN STRUCTURE

We expect that our method will help to clarify the situation regarding predominant fiber orientations in cartilage tissue where they are arranged in a complicated 3-D manner. Given the need to improve the precision of the quantitative 3-D method noted above, initially we have investigated the structure of cartilage in a semi-qualitative manner. Eq. (8) shows that, for a given n_e and n_o, the smaller the Δn the smaller the angle between the light propagation direction and the c-axis. By observing whether the apparent birefringence is greater or smaller or roughly equal for incidence angles that are symmetrically placed about normal incidence, we have constructed a qualitative map of dominant c-axis orientation as follows.

In subsequent sections we will refer to two orthogonal planes in the tissue. The plane containing the sagittal ridge is the "sagittal plane" while the "coronal plane" is orthogonal to this but also contains the long-axis of the bone shaft. Referring to Fig. 6 we see that these two planes divide the half-space lying above the joint surface into four octants. Labeling directions lying in these planes as A, P, M and L (meaning directions in the anterior, posterior, medial or lateral direction), then we can label these octants as AM,

Table II

Tendon experiments comparing results obtained by the method used in Table I with the method based on Eq. (4). The last row reports results for the data shown in Fig. 4, i.e., where the method used in Table I cannot be applied, due to the absence of a complete retardance band

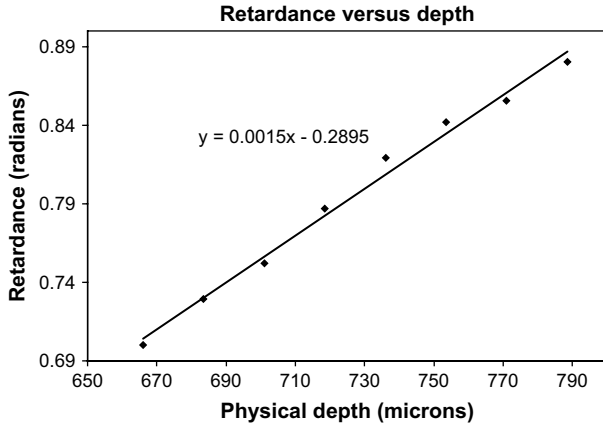| $\theta_{nominal}$ (°)	$\varphi_{nominal}$ (°)	$\theta_{derived}$ (°)	$\varphi_{derived}$ (°)	$n_e - n_o$	$\theta_{derived}$ (°)	$\varphi_{derived}$ (°)	$n_e - n_o$
			Δn from band-spacing			Δn from retardance gradient	
90	0	85	0	5.1×10^{-3}	96	−9	2.2×10^{-3}
20	0	n/a	n/a	n/a	23	0	3×10^{-3}

Retardance versus depth

$y = 0.0015x - 0.2895$

Fig. 5. Illustrative curve of retardance vs physical depth extracted from the bottom-left image in Fig. 4.

AL, PM and PL (for anterior−medial, etc.). For PS-OCT scanning we arrange the joint surface such that the sagittal plane is aligned with the laboratory vertical. We then illuminate a fixed point on the sample with five illumination directions as follows: direction '0' is normal to the surface, 'v1' and 'v2' are directions confined to the laboratory vertical plane and symmetrically oriented about the surface normal with incident angles $+35°$ and $-35°$ whilst 'h1' and 'h2' are the equivalent directions lying in the laboratory horizontal plane. Then for each of these five illumination directions we obtain PS-OCT retardance images and qualitatively score the birefringence on a five-point scale of increasing
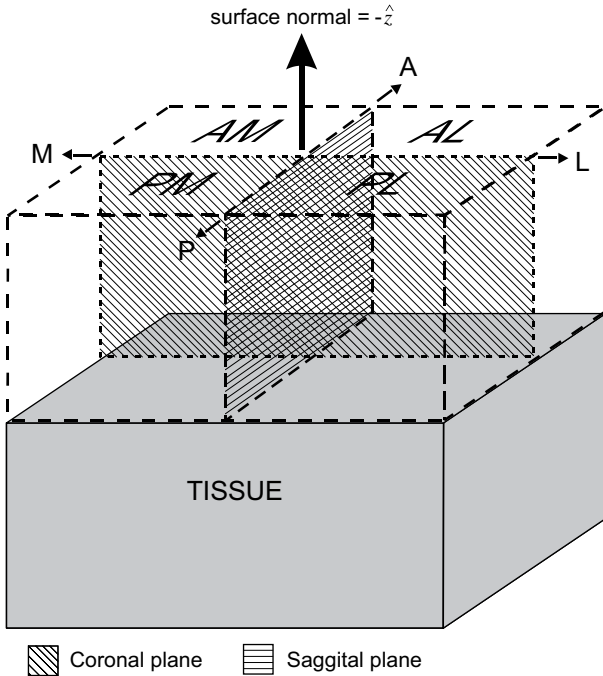
surface normal = -$\hat{z}$

Fig. 6. Illustrating the sagittal and coronal planes in relation to the tissue surface normal and also the anterior, posterior, lateral and medial directions (A, P, L, M, respectively). These planes divide up the tissue into four octants AM, PM, AL, PL, respectively, each of which represents a unique 3-D *c*-axis orientation that can be inferred using the semi-qualitative method described in the text.

Table III
Illustrating how the qualitative five-point scoring of apparent birefringence, obtained using five illumination directions, can be used to infer the approximate orientation of the fiber c-*axis in 3-D space. This semi-qualitative method is used to analyze the cartilage data*

	0	h1	h2	v1	v2
N	—	**	**	**	**
A → P	****	****	****	**	**
AM	**	*	***	*	***
SA	**	**	**	*	***

birefringence, denoted by the symbols $(-, *, **, ***, ****)$ where for example '$-$' denotes the absence of observable birefringence. Then we can ascribe a qualitative 3-D *c*-axis orientation to the *c*-axis as follows. Imagine projecting the *c*-axis out of the tissue and up into the positive half-space. If the location of the distal end of this vector lies in the octant 'AM' then we denote this orientation as AM, indicating a polar tilt and also an azimuthal orientation into octant AM. If the *c*-axis lies parallel to the surface and also in the sagittal plane then we denote this as A → P. If the *c*-axis has a polar tilt and is confined to the sagittal plane, such that the distal end of the vector is directed toward the anterior, then we denote this as SA. If the vector points parallel to the surface normal then we denote this as N. In total there are 13 such directions. Table III tabulates a subset of these and shows how the qualitative birefringence score for the five illumination directions has a unique pattern for each 3-D orientation, in terms of the symmetry/asymmetry and absolute values of the Δn values obtained for each direction. In this way we obtain a qualitative 3-D mapping of cartilage. The only serious restriction of this approach occurs when the fibers lie in the plane of the surface (i.e., $\theta = 90°$). In this case it is not possible to determine the position of the *c*-axis uniquely as its position can be mirrored in the sagittal or coronal plane and still produce the same apparent birefringence. However, this situation is readily handled by determining the fast-axis orientation using phase-resolved methods[26] (although we have not done that in this report).

We first collected PS-OCT images taken at anterior and posterior sites with illumination directions lying in the coronal plane. At each point, a sequence of measurements was made in the two orthogonal planes, with equal but opposite illumination angles. For all locations and angles 4 mm wide by 1 mm deep retardance images were acquired. Fig. 7. shows the results. PS-OCT images from the posterior region (upper row) showed similar retardance images for equal and opposite polar angles of illumination (left and right columns), with no distinct retardance bands visible. On the other hand, results for anterior part (lower row) show a clear asymmetry, with a distinctive retardance band visible for illumination direction $-35°$, but not for $+35°$. This means that in the posterior region the apparent birefringence is low for both illumination directions but in the anterior region is markedly higher for the negative illumination direction. In earlier studies, we collected PS-OCT images taken at these same sites with illumination directions lying in the sagittal plane[16]. From these previous studies we inferred that at these sites the dominant *c*-axis has a polar angle oriented as shown in Fig. 8. Combining this information with that obtained from the coronal plane, we infer that the fiber long-axis lies approximately in the plane parallel to sagittal ridge in the posterior region. In the anterior region the data suggest that the fiber's long-axis is inclined toward
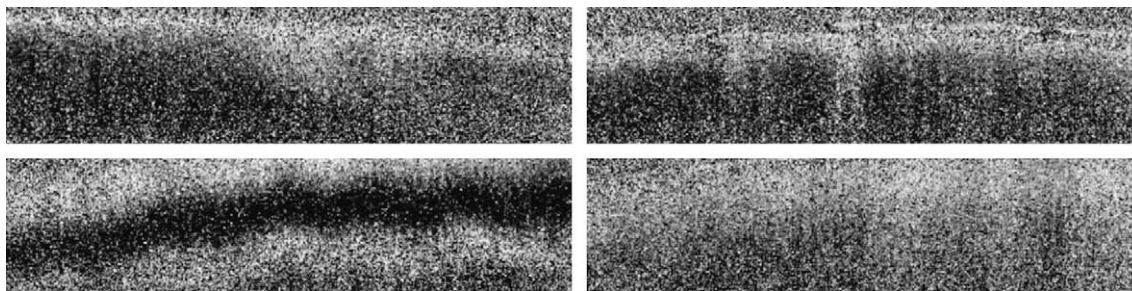
Fig. 7. Retardance images obtained at a point on the posterior surface of the condyle (top row) and anterior (bottom row), using angles of incidence in air of $-35°$ (left) and $+35°$ (right), where a negative angle signifies that the beam propagates from the margin toward the sagittal ridge. The tissue surface is at the top of the image, but the air above the surface appears as gray noise rather than a dark region, because A_v and A_h are zero in this region and so the retardance is then calculated as the ratio of two noisy quantities. Note the approximately symmetric appearance of the retardance images in the posterior region but the marked asymmetry for the anterior region, with a clear retardance band visible using an angle of incidence in air of $-35°$.

the internal part of the joint, i.e., in the direction of sagittal ridge, as shown schematically in Fig. 9. These results suggest a complicated 3-D structure for the collagen fiber orientation in the radial layers of the cartilage.

To gain confidence that such variations in fiber orientations genuinely exist and are not spurious artefacts, independent assessments were made using the established techniques of split-line analysis and polarized light micrographs. Firstly, an intact metacarpophalangeal joint was pricked with a needle dipped in India ink. Figure 10 shows the anterior surface of the joint, with the ridge to the left and the apex toward the top. Note the similarity between the azimuthal orientation of the fibers in the superficial layer and that suggested by PS-OCT for the deeper regions (Fig. 9). Figure 11 shows a pair of polarized light micrographs, obtained from the metacarpophalangeal joint. Samples of bone with cartilage attached were cut while frozen into 20 μm thick coronal sections. Images collected from sites at each end of the slice, separated by about 1 cm, are shown in the figure. These images clearly demonstrate that the preferred orientation of chondrocyte cells, and by implication the collagen matrix, is highly changeable on cm length scales.

To study collagen fiber orientation further, we collected a series of OCT images along a line to the anterior side of the apex, extending from close to the sagittal ridge to the margin (Fig. 12). This area is of interest as it is subjected to high loading yet rarely demonstrates osteochondral lesions[27]. Sequences of angle-resolved measurements were made for three spots along that line (Fig. 13). Rows 1–3 correspond to points 1–3, respectively. For all locations and angles, 4 mm long images were acquired.

Images for equal and opposite polar angles show inverse appearance of retardation bands. At site 1 there are retardation bands for positive polar angles of illumination but at the third site a banded retardation image arises for negative polar illumination angle. This implies that the polar angle of the fibers changes as one moves from the ridge toward the margin, as shown schematically in Fig. 14. This "twist effect" of collagen fiber polar orientation at points along the apex in articular cartilage may be related to in vivo load distributions. A detailed investigation of the 3-D collagen fiber orientation through the whole area of articular cartilage, therefore, appears to be justified.

Discussion

We have described a novel optical technique to determine 3-D structural information concerning collagen alignment in intact articular cartilage. The method is rapid, non-destructive and offers good penetration (1–2 mm) into intact tissue. It could potentially be applied in vivo during arthroscopy or as a monitoring tool in a bioreactor. This report introduces the basic concept and produces qualitative maps of the dominant fiber orientation in cartilage based on measurements of apparent optical birefringence using multiple illumination directions in two orthogonal planes. This work further suggests that this structure is non-trivial, with site-to-site variations in polar and azimuthal angles for the collagen in the radial zone. The work is, however, merely a starting point and the method has, we believe, significant potential for improvement.

Firstly the quantitative application of our method to tendon uses the simplest method of determining the apparent birefringence Δn, which is to measure the band-spacing

Fig. 8. Reproduced from Ref. 16 shows the dominant c-axis polar orientation inferred by comparing Δn values for different illumination directions that are confined to the sagittal plane (retardance images not shown).
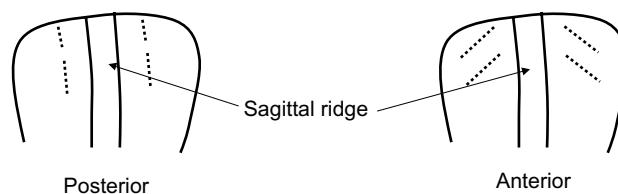

Fig. 9. Schematic diagram of the apparent variation in azimuthal orientation of type-II collagen fibers of the equine fetlock joint on the posterior and anterior surfaces. Coronal view: the joint apex is at the top of each diagram.
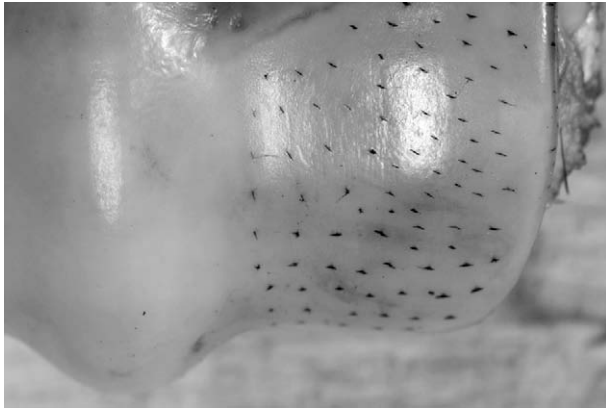
Fig. 10. The anterior surface of a condyle after performing a split-line experiment. The apex is at the top of the photograph. The general fiber alignment suggested by destructive testing of the superficial layer is in qualitative agreement with the alignment suggested by non-destructive PS-OCT of the deeper layers.

Fig. 12. Schematic of the condyle (sagittal ridge in gray), with the three measurement sites on the anterior side of the apex labeled 1–3.

in the retardance images. However, this method of estimating Δn restricts quantitative application to tissues with high Δn. Since tissues such as cartilage and meniscus have lower Δn[28] our reported results for cartilage are qualitative. However, more sophisticated methods exist for calculating Δn, e.g., calculating the slope of retardance vs distance or using Jones matrix/Stokes-vector approaches. These methods do not require the presence of a complete birefringence band and so an interesting area for further development is to apply these approaches to the quantitative mapping of cartilage structure.

Secondly, measurement of apparent birefringence in two orthogonal planes is experimentally cumbersome and likely to be difficult to perform *in vivo* during an arthroscopy. More fundamentally, the two planes of imaging obviously do not overlap in 3-D space, which means the tissue must have broadly uniform collagen organization over an area of a few square millimeters, so that the data from the two planes can meaningfully be combined. However, in this report we have only used part of the information available from PS-OCT, namely the apparent birefringence. PS-OCT can also provide information on the apparent fast-axis orientation[26,29]. A formalism exists, the extended Jones matrix calculus, to relate both quantities to the absolute
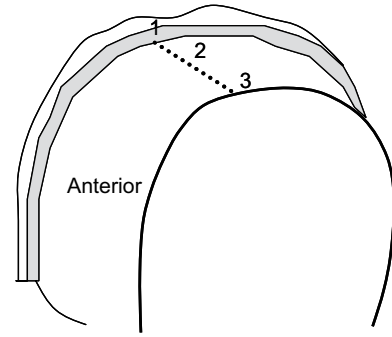
3-D *c*-axis orientation[25], so that it should be possible to extract the desired information using illumination directions confined to a single-plane[30].

Thirdly, PS-OCT intrinsically yields depth-resolved information so that the rather qualitative picture of collagen orientation in the radial zone presented here could be refined considerably. There have been several reports in which the fast-axis orientation of birefringent tissues has been inferred as a function of depth for muscle and intervertebral disk. This approach typically uses a more sophisticated PS-OCT system than that used in our study, in which the incident polarization state is modulated and the back-scattered polarization state analyzed in order to infer the depth-resolved Jones matrix of the sample. By combining these approaches with multiple illumination directions it should be possible to determine the 3-D structure of the superficial and radial zones independently and also infer the extent of the transitional zone, as the random orientation of fibers in this region should manifest itself as a region with very low apparent birefringence for all illumination directions[18]. The development of such an algorithm is an ongoing project in our laboratory. Further results will be reported in due course.

The ability to determine the 3-D structure of cartilage collagen non-destructively and rapidly has a number of potential applications. Firstly it would allow a complete characterization of normal joints and allow one to relate fiber morphology to *in vivo* load distributions. Secondly, the
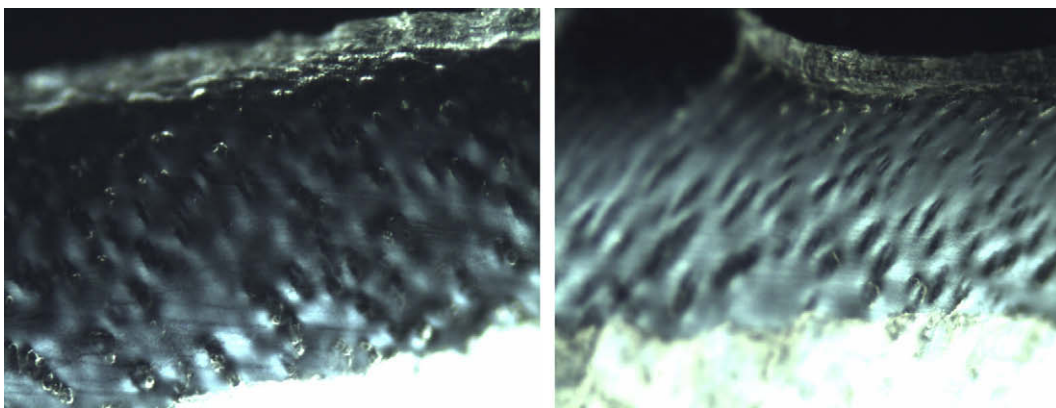

Fig. 11. Polarized light micrographs obtained from each end of a 1.5 cm coronal cartilage section. Clear differences in the directional alignment are evident over cm length scales, lending support to the indications from PS-OCT.
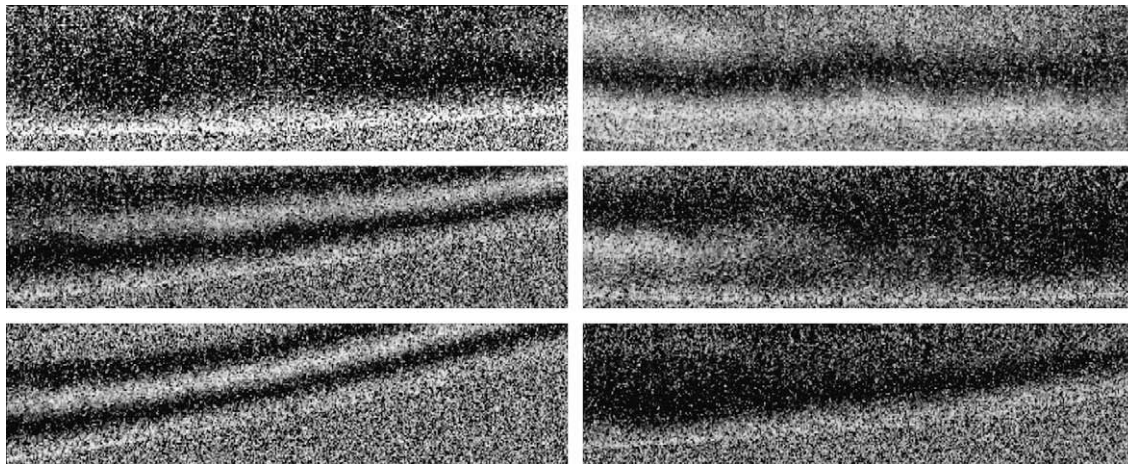
Fig. 13. Retardance images obtained at the points 1−3 are shown in rows 1−3, respectively (the tissue surface is toward the bottom of the images). The left column is a 4 × 1 mm sagittal section image taken with the illumination beam inclined in the sagittal plane by an angle of 40° toward the posterior side of the joint (i.e., the beam travels from the posterior toward the anterior: defined as −40°) while the right column shows the corresponding image obtained with an equal and opposite positive angle of illumination, i.e., inclination toward the anterior side.

production of a tissue-engineered construct to replace damaged cartilage at a particular site could then include site-specific information when determining the appropriate scaffold geometry needed to promote correctly oriented collagen *in situ*. Thirdly, the implanted construct could be monitored arthroscopically and the degree to which collagen had correctly regenerated could be quantitatively studied. Finally, basic biomechanical data concerning the properties of cartilage could be obtained by exploiting the near real-time data acquisition speed of PS-OCT. Since PS-OCT is non-contact, one could envisage an experiment in which cartilage is dynamically loaded over physiologically relevant time-scales (e.g., to match load-bearing exercise) and the dynamic reorientation of the fibers in 3-D space monitored.

In summary, variable-incidence angle PS-OCT has the potential to become a tool with unique capabilities for studying the collagen structure of intact articular cartilage. The prospects of improved tissue-engineered constructs and the quantitative assessment of ECM production *in situ* should act as a powerful stimulus to fully develop the method.
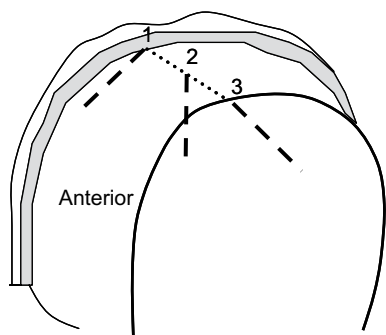
Conflict of interest

The authors declare that there are no conflicts of interest affecting the publication of this manuscript.

Fig. 14. The dominant polar orientation of collagen fibers at the measurement sites 1−3, as suggested by the asymmetric retardance images shown in Fig. 9. At point 1, nearest the sagittal ridge, the fibers are directed toward the anterior. This orientation changes to being directed toward the posterior at the point nearest the margin.

References

1. Nesic D, Whiteside R, Brittberg M, Wendt D, Martin I, Mainil-Varlet P. Cartilage tissue engineering for degenerative joint disease. Adv Drug Deliv Rev 2006;58:300−22.
2. Beris AE, Lykissas MG, Papageorgiou CD, Georgoulis AD. Advances in articular cartilage repair. Injury 2005;36:S14−23.
3. Glaser C, Putz R. Functional anatomy of articular cartilage under compressive loading: quantitative aspects of global, local and zonal reactions of the collagenous network with respect to the surface integrity. Osteoarthritis Cartilage 2002;10:83−99.
4. Wilson W, Driessen NJB, van Donkelaar CC, Ito K. Prediction of collagen orientation in articular cartilage by a collagen remodeling algorithm. Osteoarthritis Cartilage 2006;14:1196−202.
5. Hültkrantz W. Über die Spaltrichtungen der Gelenkknorpel. Verh Anat Ges 1898;12:248−56.
6. Moger CJ, Barrett R, Bleuet P, Bradley DA, Ellis RE, Green EM, *et al.* Regional variations of collagen orientation in normal and diseased articular cartilage and subchondral bone determined using small angle X-ray scattering (SAXS). Osteoarthritis Cartilage 2007;15:682−7.
7. Meder R, de Visser SK, Bowden JC, Bostrom T, Pope JM. Diffusion tensor imaging of articular cartilage as a measure of tissue microstructure. Osteoarthritis Cartilage 2006;14:875−81.
8. Wolman M, Kasten FH. Polarized light microscopy in the study of the molecular structure of collagen and reticulin. Histochemistry 1986; 85:41−9.
9. Bi X, Li G, Doty SB, Camacho NP. A novel method for determination of collagen orientation in cartilage by Fourier transform infrared imaging spectroscopy (FT-IRIS). Osteoarthritis Cartilage 2005;13:1050−8.
10. de Boer JF, Milner TE, van Gemert MJC, Nelson JS. Two-dimensional birefringence imaging in biological tissue by polarization sensitive optical coherence tomography. Opt Lett 1997;22(12):934−6.

11. Herrmann JM, Pitris C, Bouma BE, Boppart SA, Jesser CA, Stamper DL, *et al.* High resolution imaging of normal and osteoarthritic cartilage with optical coherence tomography. J Rheumatol 1999;26:627−35.

12. Jiao SL, Yu WR, Stoica G, Wang LHV. Contrast mechanisms in polarization-sensitive Mueller-matrix optical coherence tomography and application in burn imaging. Appl Opt 2003;42(25):5191−7.

13. Drexler W, Morgner U, Ghanta RK, Kartner FX, Schuman JS, Fujimoto JG. Ultrahigh-resolution ophthalmic optical coherence tomography. Nat Med 2001;7(4):502−7.

14. Yang Y, Dubois A, Qin XP, Li J, El Haj A, Wang RK. Investigation of optical coherence tomography as an imaging modality in tissue engineering. Phys Med Biol 2006;51(7):1649−59.

15. Han CW, Chu CR, Adachi N, Usas A, Fu FH, Huard J, *et al.* Analysis of rabbit articular cartilage repair after chondrocyte implantation using optical coherence tomography. Osteoarthritis Cartilage 2003;11:111−21.

16. Ugryumova N, Attenburrow DP, Winlove CP, Matcher SJ. The collagen structure of equine articular cartilage, characterized using polarization-sensitive optical coherence tomography. J Phys D Appl Phys 2005;38:2612−9.

17. Yeh P. Optical Waves in Layered Media. New York: Wiley; 1988.

18. Oldenbourg R, Ruiz T. Birefringence of macromolecules. Wiener's theory revisited, with applications to DNA and tobacco mosaic virus. Biophys J 1989;56(1):195−205.

19. Ugryumova N, Gangnus SV, Matcher SJ. Three-dimensional optic axis determination using variable-incidence-angle polarization optical coherence tomography. Opt Lett 2006;31:2305−7.

20. de Boer JF, Milner TE. Review of polarization sensitive optical coherence tomography and Stokes vector determination. J Biomed Opt 2002;7(3):359−71.

21. Matcher SJ, Winlove CP, Gangnus SV. The collagen structure of bovine intervertebral disc studied using polarization sensitive optical coherence tomography. Phys Med Biol 2004;49:1295−306.

22. Sorin WV, Baney DM. A simple intensity noise reduction technique for optical low-coherence reflectometry. IEEE Photonics Technol Lett 1992;4:1404−6.

23. Izatt JA, Kulkarni MD, Yazdanfar S, Barton JK, Welch AJ. *In-vivo* bidirectional color Doppler flow imaging of picoliter blood volumes using optical coherence tomography. Opt Lett 1997;22(18): 1439−41.

24. Hee MR, Huang D, Swanson EA, Fujimoto JG. Polarization-sensitive low-coherence reflectometer for birefringence characterization and ranging. J Opt Soc Am B 1992;9:903−8.

25. Gu C, Yeh P. Extended Jones matrix method. II. J Opt Soc Am A 1993; 10(5):966−973.

26. Hitzenberger CK, Gotzinger E, Sticker M, Pircher M, Fercher AF. Measurement and imaging of birefringence and optic axis orientation by phase resolved polarization sensitive optical coherence tomography. Opt Express 2001;9(13):780−90.

27. Brama PAJ, Karssenberg D, Barneveld A, van Weeren PR. Contact areas and pressure distribution on the proximal articular surface of the proximal phalanx under sagittal plane loading. Equine Vet J 2001;33(1):26−32.

28. Xie T, Guo S, Zhang J, Chen Z, Peavy GM. Determination of characteristic of degenerative joint diseases using optical coherence tomography and polarization sensitive optical coherence tomography. Lasers Surg Med 2006;38:852−65.

29. Kemp NJ, Zaatari HN, Park J, Rylander HG, Milner TE. Depth-resolved optic axis orientation in multiple layered anisotropic tissues measured with enhanced polarization-sensitive optical coherence tomography (EPS-OCT). Opt Express 2005;13(12):4507−18.

30. Ugryumova N, Gangnus SV, Matcher SJ. Variable-angle-of-incidence polarization-sensitive optical coherence tomography: its use to study the 3-D collagen structure of equine articular cartilage. Proc Soc Photo Opt Instrum Eng 2006;6079:60792C−1.